

Article

Numerical Analysis of Modified PVA Fiber Rubber Concrete in Frame Beams

Lijuan Li ^{1,2}, Fang Xing ³, Zhijun Xu ^{1,2,*}, Wang Chen ¹, Wuxin Chen ¹ and Yongquan Li ¹

¹ College of Civil Engineering and Architecture, Henan University of Technology, Zhengzhou 450001, China
² Henan International Joint Laboratory of Modern Green Ecological Storage System, Zhengzhou 450001, China
³ Department of Hydraulic Engineering, Henan Vocational College of Water Conservancy and Environment, Zhengzhou 450008, China
* Correspondence: xuzhijun@haut.edu.cn

Abstract: The feasibility of PVA fiber rubber concrete modified by modifier in the structure was investigated using the portal frame as the research object. The basic mechanical properties of modified PVA rubber concrete materials were tested mechanically first, and then ABAQUS was used to establish the ordinary concrete portal frame model, and after confirming the model's rationality, the rubber concrete, PVA rubber concrete, and modified PVA rubber concrete models were established on this basis, and the displacement and strain comparison analysis with ordinary concrete was carried out. The simulation results show that using PVA rubber concrete material in the concrete frame structure can improve the large deformation of rubber concrete, and using PVA rubber concrete treated with a modifier can improve structural strength and deformation even more.

Keywords: PVA fiber rubber concrete; modifiers; frame structure; numerical simulation



Citation: Li, L.; Xing, F.; Xu, Z.; Chen, W.; Chen, W.; Li, Y. Numerical Analysis of Modified PVA Fiber Rubber Concrete in Frame Beams. *Buildings* **2023**, *13*, 791. <https://doi.org/10.3390/buildings13030791>

Academic Editor: Marco Di Ludovico

Received: 1 February 2023
Revised: 7 March 2023
Accepted: 11 March 2023
Published: 17 March 2023



Copyright: © 2023 by the authors. Licensee MDPI, Basel, Switzerland. This article is an open access article distributed under the terms and conditions of the Creative Commons Attribution (CC BY) license (<https://creativecommons.org/licenses/by/4.0/>).

1. Introduction

Rubber concrete is a new type of recycled environmental protection building material that uses regular concrete as the matrix and waste rubber granules to improve the impact resistance [1], impermeability [2], heat insulation and sound insulation [3], and fatigue resistance [4] of ordinary concrete while also resolving the issue of land occupation and environmental pollution of waste tire rubber [5]. It also has good application benefits [6]. Current research is focused on finding ways to increase the toughness of concrete and lessen strength loss while employing waste rubber because the incorporation of waste rubber weakens some of the mechanical qualities of rubber concrete [7]. In order to create high-performance fiber-reinforced cementitious composites (HPFRCC), many researchers have added fiber materials as toughening materials [8] to concrete. These composites have high ductility [9], high toughness [10], and significant multi-crack cracking characteristics, which can effectively balance the contradiction between the strength and brittleness of regular concrete. To get superior particular qualities while lowering costs and maximizing economic benefits, several academics have suggested that fibers and rubber be added to concrete [11]. Several academics approach the issue using theoretical analysis [12], laboratory tests [13–17], and numerical simulation [18–20]. ABAQUS is a finite element engineering simulation program that can investigate challenging nonlinear issues [21].

Jiaqing Wang [22] assessed the compressive and flexural resistance, alkali-silicon reaction (ASR) expansion, drying shrinkage, and freeze-thaw resistance of polyvinyl alcohol (PVA) fiber-reinforced rubber concrete. The results showed that the rubber concrete added with PVA fiber could improve the elongation and fracture energy of the specimen after cracking, and the resistivity test results showed that the permeability of PVA was increased. Yong Feng [23] examined the mechanical properties of concrete containing different amounts of PVA rubber through mechanical tests. The complete process, from integrity to damage to cracking, was then simulated using a mesoscopic numerical model of PVA

rubber and concrete. This demonstrated the mesoscopic finite element model's precision. It provides a theoretical framework for the structural numerical simulation analysis and design of this form of concrete. Weijian Wang [24] believed the connection between the PVA fiber and the rubber particles was weak, so he chose to add a KH560 modifier to strengthen the PVA/rubber concrete interface. The efficacy of the additive was then assessed using compression, shear, fracture, scanning electron microscope (SEM), and infrared spectrum (FTIR) tests, and it was found that it could strengthen the weak adhesion at the PVA/rubber concrete contact. Based on past experience, we believe PVA fiber-reinforced rubber concrete can improve the ductility and durability of the construction. Due to the tenuous connection between the PVA fiber and the rubber particles, the modifier KH560 is first applied to the fiber.

The use of rubber concrete in frame structures has received relatively little attention. Through the pseudo-static test of columns and the normal section bending test of beams, Yue Li [25] et al. investigated the structural properties of reinforced rubber concrete members and contrasted them with the pertinent characteristics of regular concrete members. The effects of adding rubber aggregate to the beam on the seismic performance of the frame-shear wall construction were theoretically examined by Haoran Li [26] et al. Through model tests, Houmin Li [27] examined how the use of rubber concrete affected the bearing capacity and deformation of reinforced concrete structures using the door frame as the study object. Rubber concrete is not frequently utilized in concrete structures because it loses strength. We selected the PVA fiber-reinforced rubber concrete modified by KH560 to test its mechanical properties, studied the feasibility of the application of the modified PVA fiber-reinforced rubber concrete in the frame structure by means of numerical analysis, and discussed the rational use of KH560-modified PVA rubber concrete in structural engineering. To explore whether rational use of KH560 modified PVA rubber concrete in structural engineering can reduce the bearing capacity of structures less or even increase, we explore its feasibility in engineering application, and provide a reference for future related research.

The research flow framework is shown in Figure 1.

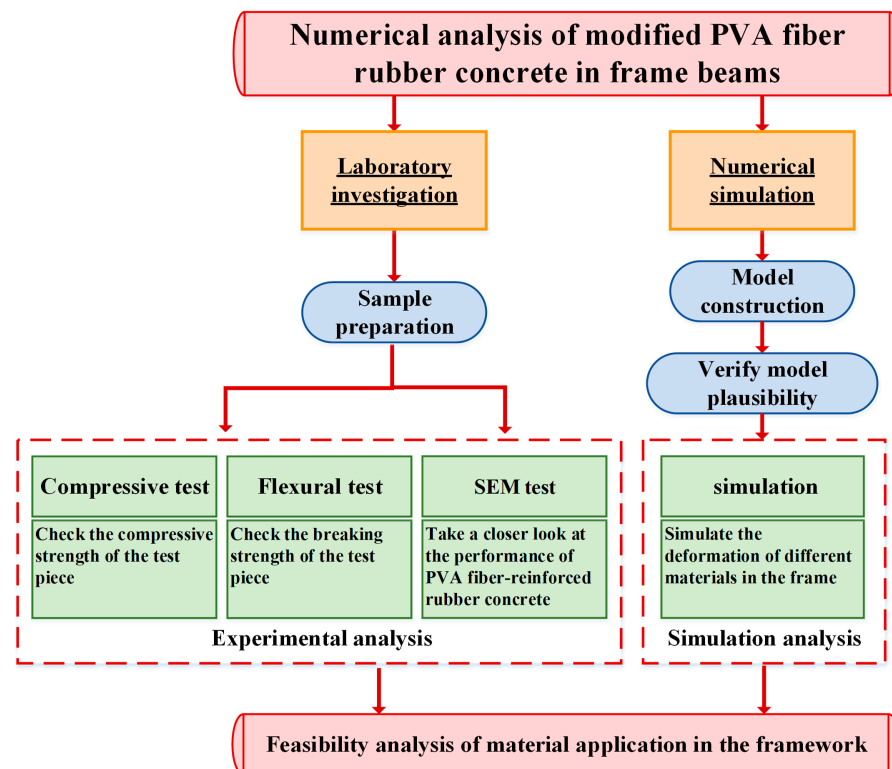


Figure 1. Flow research framework.

2. PVA Fiber Rubber Concrete Mechanical Properties Test

2.1. Test Materials

The cement in this test adopts P.O 42.5 ordinary Portland cement, and the physical and mechanical properties are shown in Table 1. The fine aggregate uses medium sand, whose fineness modulus is 5–25, and its apparent density is 2650 kg/m³ and bulk density is 1850 kg/m³. Coarse aggregate stone is a continuous gradation, whose particle size is 5–25 mm, and its apparent density is 2703 kg/m³ and bulk density is 1550 kg/m³. Rubber particles have a particle size of less than 4 mm, and Table 2 lists their fundamental characteristics. The fiber is made of polyvinyl alcohol (PVA) fiber, and Table 3 displays the fundamental performance indicators. KH560 is used as the coupling agent, and Table 4 displays its physical characteristics.

Table 1. Physical and mechanical properties of cement.

Specific Surface Area/(m ² ·kg ⁻¹)	Standard Consistency/%	Coagulation Time/min		Stability	Flexural Strength/MPa		Compressive Strength/MPa	
		Initial Setting Time	Final Setting Time		3d	28d	3d	28d
370	27	150	205	√	4.8	8.0	29.2	48.5

Table 2. Basic performance indicators of rubber particles.

Mesh	Apparent Density /kg/m ³	Bulk Density /kg/m ³	Elastic Modulus /GPa	Particle Size Range /mm	Poisson Ratio
5	1.03	610	0.07	≤4	0.449

Table 3. Basic performance index of PVA fiber.

Density/kg/m ³	Diameter/μm	Elastic Modulus /GPa	Length /mm	Tensile Strength/MPa	Break Elongation/%	Poisson Ratio
1.3	15	39	6	1704	12	0.3

Table 4. Physical properties of KH-560 coupling agent.

Type	Density/kg/m ³	Chromatographic Purity/%	Boiling Point/°C	Refractive Index/ND25	Flash Point/°C
KH560	950	97.5	290	1.426	110

2.2. Test Mix Ratio

Refer to JGJ55-2011 “Design Regulations for Ordinary Concrete Mix Ratio” to determine the concrete mix ratio. The primary research factor used in the specimen design is PVA dose. The water–cement ratio for the ordinary concrete (PC) specimen is 0.42, and it is designed for the strength class C25. RC stands for rubber particle replacement rate, which was set at 20% and designated as RC20. Rubber particles were injected in a method that replaced fine aggregate by an equal volume. PVA0.5, PVA1.0, and PVA1.5 denote the volume fraction of PVA as 0.5vol%, 1.0vol%, and 1.5vol%, respectively. PVA and KH560 reflect the content of PVA fiber and KH560. KH560 has a fixed replacement rate of 1.5 percent. As illustrated in Table 5, the mixing ratio for six groups of PVA fiber rubber concrete is designed.

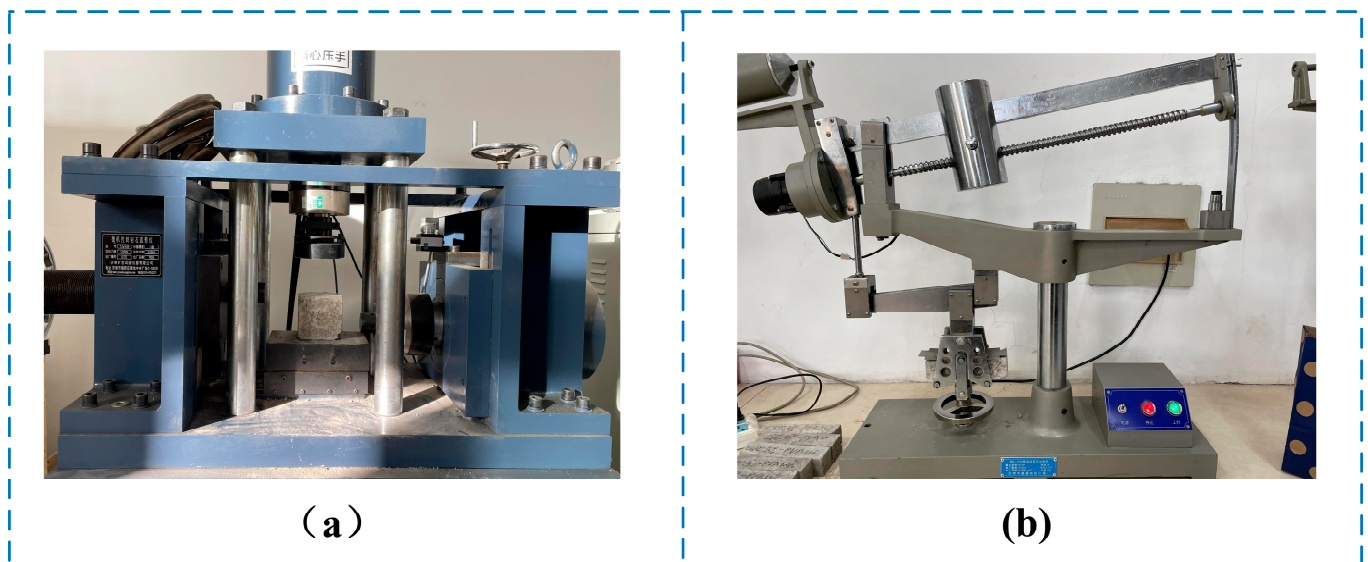
Table 5. Modified PVA fiber rubber concrete mix ratio.

Name	Cement /kg	Water/kg	Fine Aggregate /kg	Coarse Aggregate /kg	Rubber Particles/kg	PVA /g	KH560 /g
PC	416	175	593	1260			
RC20	416	175	474	1260	39.1		
RC20-PVA0.5	416	175	474	1260	39.1	19.4	
RC20-PVA1.0	416	175	474	1260	39.1	38.6	
RC20-PVA1.5	416	175	474	1260	39.1	57.8	
RC20-PVA1.0-KH560	416	175	474	1260	39.1	38.6	2.67 g

Notes: PC—Plain concrete; RC—Rubber particles; PVA—PVA fiber; RC20—Rubber volume substitution ratios of 20%; PVA0.5%, PVA1.0%, PVA1.5%—PVA fiber volume fractions of 0.5vol%, 1.0vol%, and 1.5vol%, respectively; KH560—KH560 modifier volume fractions of 1.5vol%.

2.3. Test Method

Y250 digital display electro-stress type direct shear instrument was used as loading equipment for the compression test, as shown in Figure 2a. The breaking test equipment adopts DKZ-5000 electric bending tester, as shown in Figure 2b. We designed 1 group of PC ordinary concrete specimens, 1 group of rubber/concrete specimens, 3 groups of PVA/rubber/concrete specimens, and 1 group of KH560/PVA/rubber/concrete specimens. The mix ratio is shown in Table 5. Each group had 6 cube specimens with the size of 100 mm × 100 mm × 100 mm used to measure the mean value of compressive strength and the corresponding error bars for 7 and 28 days of curing, and 6 specimens with the size of 40 mm × 40 mm × 160 mm were used to measure the mean value of breaking strength and the corresponding error bars for 7 and 28 days of curing. The specimen was demolded 24 h after casting, and cured for 7 days and 28 days under standard conditions (20 ± 2 °C, humidity $\geq 95\%$). The test process is shown in Figure 3.

**Figure 2.** Laboratory equipment: (a) Pressure device; (b) Breaking device.

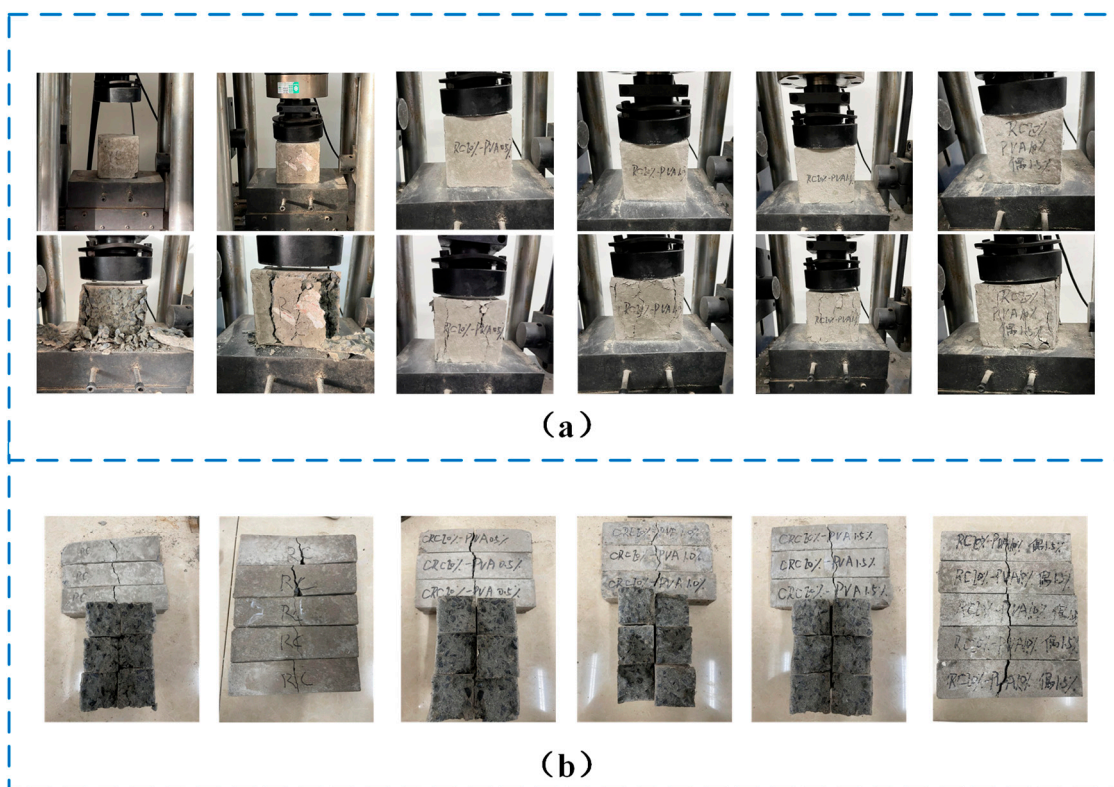


Figure 3. Compressive and flexural test process diagram of specimens under different dosages: (a) Compressive test diagram of PVA-Rubber/concrete with different dosages; (b) Flexural test diagram of PVA-Rubber/concrete with different dosages.

Scanning electron microscopy was employed in this work to examine the interface of specimens with various proportions. The target sample was cut into a 10 mm cube, polished with sandpaper of 2000 mesh, and cleaned with anhydrous ethanol using an ultrasonic cleaner, and the surface powder contaminants were eliminated. The cleaned samples were dried at 60 ± 2 °C for 5 h and then tested in the Quanta FEG series SEM equipment manufactured by Beijing Zhuoteng Technology Co., LTD.

3. Analysis of Test Results

3.1. Compression Test Results and Analysis

The 100 mm × 100 mm × 100 mm non-standard specimens used in the compressive test of concrete are compressed by the Y250 digital display electric stress direct shear instrument through the displacement loading control method, and the press needs to maintain a stable and uniform rate during the test, and the displacement control is selected for speed of 1 mm/min.

Cube compressive strength calculation formula is:

$$f_{cc} = \frac{F}{A}, \quad (1)$$

where: f_{cc} stands for concrete cube compressive strength (MPa), F stands for ultimate loads (N), and A stands for the compressed area (mm^2).

Since the test piece used a non-standard test piece, the arithmetic mean measured by the three repeated test pieces was multiplied by 0.95 as the compressive strength of the restructured test piece, and the calculation was accurate to 0.01 MPa. The compressive strength of the specimen age of 7 days and 28 days is shown in Figure 4.

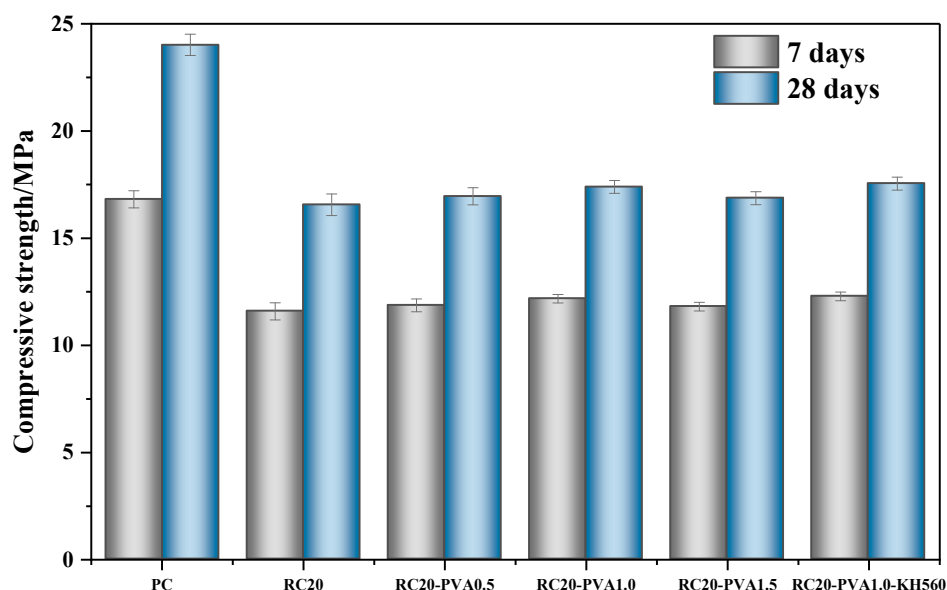


Figure 4. Compressive strength of PVA fiber rubber concrete at different dosages.

The compressive strength of the PC specimen is 24.02 MPa after 28 days, while the RC20 specimen is 16.56 MPa. RC20-PVA0.5, RC20-PVA1.0, and RC20-PVA1.5 have greater values than RC20 by 2.36%, 5.01%, and 1.87%, respectively. When compared to RC20, the compressive strength of RC20-PVA1.0-KH560 increased by 5.97%. The compressive test findings show that adding PVA to rubber concrete in the right amounts can increase its compressive strength, and adding the KH560 modifier can increase the compressive strength of PVA fiber rubber concrete even more.

3.2. Folding Test Results and Analysis

The flexural test of concrete adopts 40 mm × 40 mm × 160 mm non-standard specimens, and DKZ-5000 electric flexural testing machine is broken by the central load method, and the press needs to maintain a stable and uniform rate during the test, and record its strength when it is destroyed after the specimen is damaged.

Flexural strength calculation formula is:

$$f_f = \frac{Fl}{bh^2}, \quad (2)$$

where: f_f stands for flexural strength of concrete (MPa), F stands for maximum load (N), l stands for support spacing (mm), h stands for cross-sectional height of the specimen (mm), and b stands for specimen cross-sectional width (mm)

Since the test piece uses a non-standard test piece, the arithmetic mean measured by three repeated test pieces is multiplied by 0.85 as the flexural strength of the restructured specimen, and the calculation is accurate to 0.1 MPa. The flexural strength of 7 and 28 days of specimen age is shown in Figure 5.

The flexural strength of the PC specimen is 3.49 MPa after 28 days, while the RC20 specimen is 2.57 MPa. RC20-PVA0.5, RC20-PVA1.0, and RC20-PVA1.5 have greater strengths than RC20 by 30%, 42%, and 44%, respectively. When compared to RC20, the compressive strength of RC20-PVA1.0-KH560 increased by 64%. According to the results of the flexural tests, adding PVA in the right amount can increase the flexural strength of rubber concrete. This may be because PVA fibers bridge influence, increasing the specimen's strength. The PVA fiber rubber concrete specimen's flexure strength can be increased even further with the KH560 modifier.

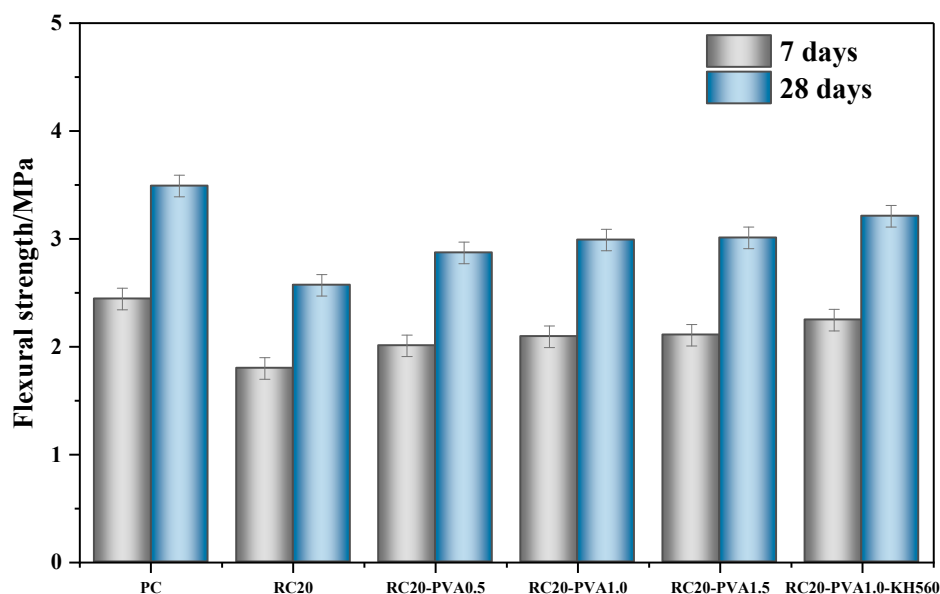


Figure 5. Flexural strength of PVA fiber rubber concrete at different dosages.

3.3. Fold Ratio

The folding ratio is the ratio of the flexural strength of the concrete material to the compressive strength of the cube, which can reflect the brittleness characteristics of the concrete material to a certain extent, and the toughness of the concrete material is better with the increase of the folding ratio, and Table 6 shows the folding ratio of each group of concrete specimens after 28 days of curing. It can be seen from the Table 6 that PVA fibers of various volume rates are added to RC, which improves the folding ratio of the material to varying degrees, the PVA fiber content is from 0 to 0.5%, 1.0% and 1.5%, the folding ratio of the specimen is increased by 9.08%, 10.76%, 14.94% compared with RC, and the folding ratio of fiber rubber concrete treated with coupling agent is increased by 6.39% compared with the same amount of fiber rubber concrete without treatment, indicating that the incorporation of PVA fiber reduces the brittleness characteristics of RC material. The toughness of the material is enhanced, and the addition of a certain amount of coupling agent can effectively improve the performance of the fiber and rubber interface transition zone, and the concrete has better crack resistance.

Table 6. Compressive and flexural strength of PVA fiber rubber concrete under different dosages.

Name	Compressive Strength/MPa	Convert Standard Strength/MPa	Flexural Strength/MPa	Convert Standard Strength/MPa	Fold Ratio
PC	25.28	24.02	4.10	3.49	0.1453
RC20	17.43	16.56	3.02	2.57	0.1552
RC20-PVA0.5	17.84	16.95	3.38	2.87	0.1693
RC20-PVA1.0	18.30	17.39	3.52	2.99	0.1719
RC20-PVA1.5	17.76	16.87	3.54	3.01	0.1784
RC20-PVA1.0-KH560	18.47	17.55	3.77	3.21	0.1829

3.4. Specimen Microstructure

Rubber is an organic material with poor compatibility with the cement matrix. It is observed in Figure 6a that the interface between the cement base and the rubber particles is almost in a state of separation, and many loose mesh structures exist in the interface, indicating that the cement base and rubber are poorly bonded, and the hydration degree of the interface is uneven, thus forming a fragile interface. The existence of the weak interface

will lead to the failure of the specimen in advance. When PVA fibers are introduced into rubber concrete, the brittleness behavior of plain concrete is eliminated to a large extent by randomly distributed fibers, and the binding force between PVA and cement mortar is also very strong under alkaline conditions. In the late failure period of PVA-rubber/concrete specimen, PVA provides three-dimensional reinforcement for the structure to resist the internal tension and inhibits the failure rate of the specimen. The strength of the rubber concrete is enhanced, and even after the cracks have penetrated the entire structure, the failed components are gathered together through the fiber bridging effect. After adding 1.5% KH-560 coupling agent, it can be obviously observed in Figure 6c that there is no obvious crack between the cement base and rubber interface, and the bond is tight, forming a continuous and uniform interface, indicating that KH-560 can significantly improve the bonding force between the cement base and rubber, and further improve the mechanical properties of PVA/ rubber concrete.

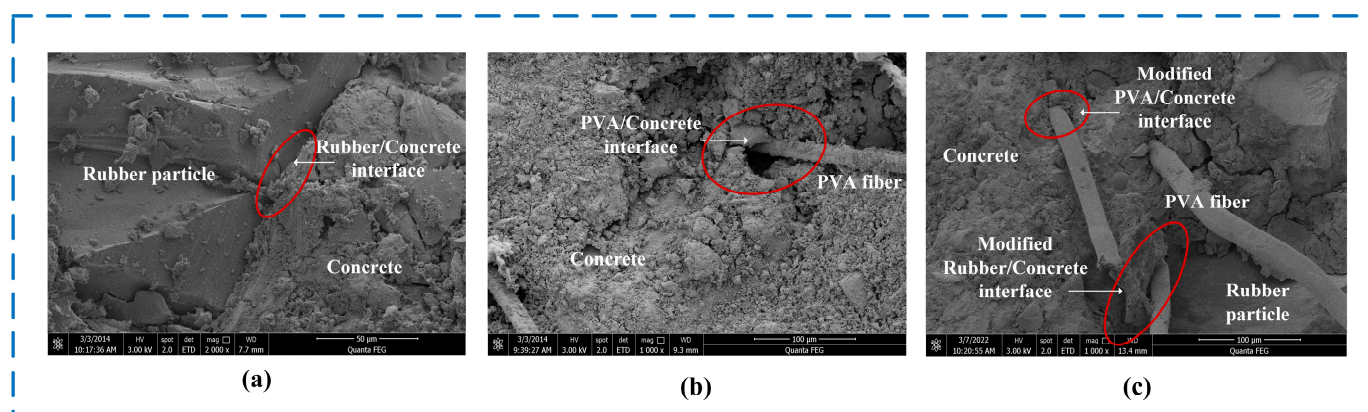


Figure 6. Micromorphology of the specimen: (a) Rubber concrete; (b) PVA-rubber/concrete; (c) KH560 modified PVA-rubber/concrete.

4. Numerical Simulation

Referring to Li Houmin's model test [27], the door frame structure was taken as the research object, the structure was 1 m long and 1 m wide, and the four materials of C25 plain concrete PC, RC20, RC20-PvA1.0, and RC20-PvA1.0-KH560 were used for numerical simulation. The structural characteristics of the particular frame are listed in Table 7, and the structural reinforcement is shown in Figure 7.

Table 7. Frame structure parameter.

Cross Section Dimension	Column Section Size	Reinforced Bar Diameter	Stirrup Diameter	Protection Cover of Reinforcing Bar
150 mm * 150 mm	150 mm * 150 mm	12 mm	8 mm	25 mm

4.1. Constitutive Relations

4.1.1. Concrete Constitutive Relations

In this paper, when the finite element simulation analysis of the frame beam of modified PVA fiber rubber concrete is carried out, the modified fiber rubber concrete is regarded as a composite material, and the relevant parameters are obtained through specific tests, and the incorporation of modified PVA fiber is expressed by changing the form of various concrete parameters.

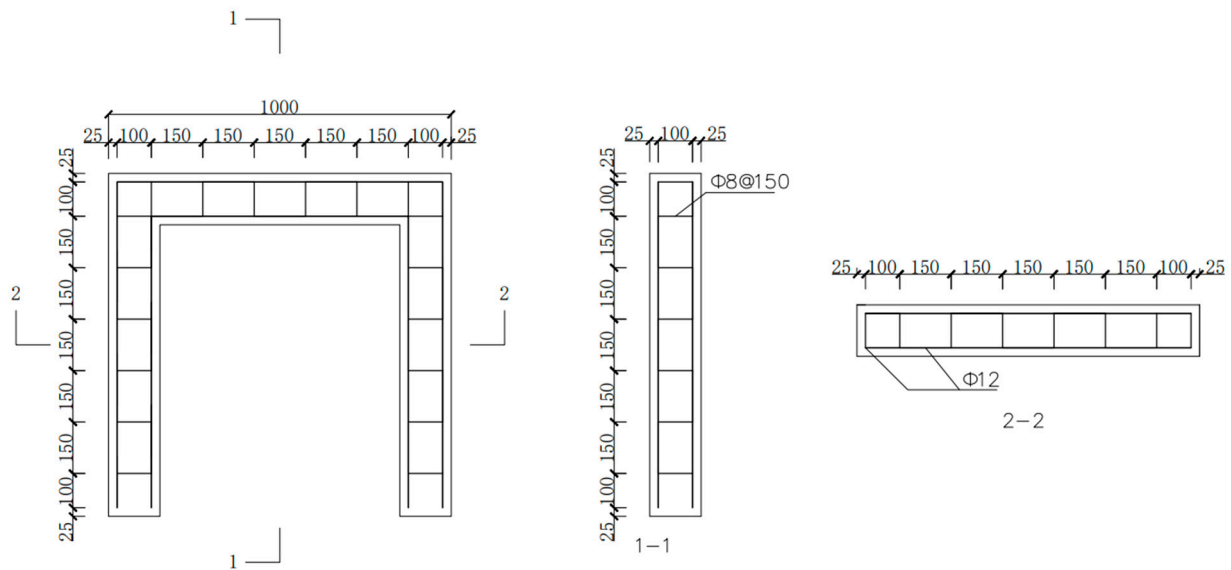


Figure 7. Reinforcement of frame structure.

The compressive stress–strain curve of modified fiber rubber concrete [28] is:

$$\sigma = (1 - d_{c,c})E_{c,c} \varepsilon, \quad (3)$$

$$d_{c,c} = \begin{cases} 1 - \frac{\rho_{c,c}n}{n-1+x^n}, & x \leq 1 \\ 1 - \frac{\rho_{c,c}n}{\alpha_{c,c}(x-1)^2+x}, & x > 1 \end{cases}, \quad (4)$$

$$\rho_{c,c} = \frac{f_{c,c}}{E_{c,c}\varepsilon_{c,c}}, \quad (5)$$

$$n = \frac{E_{c,c}\varepsilon_{c,c}}{E_{c,c}\varepsilon_{c,c} - f_{c,c}}, \quad (6)$$

$$x = \frac{\varepsilon}{\varepsilon_{c,c}}, \quad (7)$$

$$\alpha_{c,c} = \left(0.157f_{c,c}^{0.785} - 0.905\right) \left[1 - \varphi \left(14.290\lambda_r^{2.125} + 1.121\lambda_f^{1.456}\right)\right], \quad (8)$$

$$\varphi = \begin{cases} \lambda_f^{0.02}/e^{\lambda_r}, & \lambda_f \neq 0 \cap \lambda_r \neq 0 \\ 1, & \lambda_f = 0 \cup \lambda_r = 0 \end{cases}, \quad (9)$$

where: $\alpha_{c,c}$ stands for shape parameters of the descending section of the uniaxial compressive stress–strain curve of modified fiber rubber concrete, $f_{c,c}$ stands for modified fiber rubber concrete axial compressive peak stress, $\varepsilon_{c,c}$ stands for modified fiber rubber concrete corresponding peak strain, $d_{c,c}$ stands for evolution parameters of uniaxial compression damage of modified fiber rubber concrete, $E_{c,c}$ stands for modulus of elasticity of modified fiber rubber concrete (MPa), λ_r stands for rubber characteristic parameters, λ_f stands for PVA fiber characteristic parameters, and φ stands for the synergistic parameters of rubber and PVA fibers.

Tensile stress–strain curve of modified fiber rubber concrete [29] is:

$$\sigma = 1 - d_{tc}E_{cc}\varepsilon, \quad (10)$$

$$d_{tc} = \begin{cases} 1 - \rho_{tc} [1.2 - 0.2x^5], & x \leq 1 \\ 1 - \frac{\rho_{tc}}{\alpha_{tc}(x-1)^{1.7}+x}, & x > 1 \end{cases}, \quad (11)$$

$$\rho = \frac{f_{tc,r}}{E_{cc}\varepsilon_{tc,r}}, \quad (12)$$

$$x = \frac{\varepsilon}{\varepsilon_{tc,r}}, \quad (13)$$

$$\alpha_{tc} = 0.312f_{tc,r}^2 / (1 + 36\lambda_f), \quad (14)$$

$$f_{tck} = f_{cck} / (10.13 + 0.05 \times f_{cck} - 0.5\lambda_f), \quad (15)$$

$$\varepsilon_{tc,r} = f_{tc,r}^{0.54} \times 65 \times (1 + 0.2\lambda_f) \times 10^{-6}, \quad (16)$$

where: α_{tc} stands for shape parameters of the descending section of the uniaxial tensile stress-strain curve of modified fiber rubber concrete, f_{tck} stands for modified fiber rubber concrete tensile strength peak stress and corresponding peak strain, and d_{tc} stands for evolution parameters of uniaxial tensile damage of modified fiber rubber concrete.

4.1.2. Rebar Constitutive Relationship

In this paper, the rebar constitutive adopts the most widely used double-fold stress-strain constitutive relationship in finite elements, which is:

$$\sigma_p = \begin{cases} E_s \varepsilon_s, & \varepsilon_s \leq \varepsilon_y \\ f_{y,r} + k\varepsilon_s - \varepsilon_y, & \varepsilon_y < \varepsilon_s \leq \varepsilon_u \\ 0, & \varepsilon_s > \varepsilon_u \end{cases}, \quad (17)$$

$$\varepsilon_y = f_{y,r} / E_s, \quad (18)$$

$$\varepsilon_u = f_{st,r} / E_s, \quad (19)$$

$$k = (f_{st,r} - f_{y,r}) / (\varepsilon_u - \varepsilon_{uy}), \quad (20)$$

where: E_s stands for the elastic modulus of the rebar (MPa), ε_s stands for the rebar strain, $f_{y,r}$ stands for the yield strength representative value of the rebar, ε_y stands for the yield strain of the reinforcement corresponding to $f_{y,r}$, $f_{st,r}$ stands for the ultimate strength representative value of the rebar, ε_u stands for peak strain of reinforcement corresponding to $f_{st,r}$, ε_{uy} stands for the rebar hardening starting point strain, and k stands for the slope of the rebar hardening section.

4.1.3. Concrete Plastic Damage Model

There are three commonly used concrete constitutive models in ABAQUS software: the Cracking Model for Concrete (CMC), the Concrete Smeared Cracking (CSC), and the Concrete Damage Plasticity (CDP). In this paper, the CDP model is to be selected, which considers the difference in tensile and compressive properties of materials, different damage factors used in tensile and compressive damage, and has good convergence, wider scope of application, and certain advantages.

When the concrete is unloaded after being tensile or compressed beyond the elastic range, if there is no damage, the stress-strain route decreases according to the elastic modulus E_0 of the original stress peak secant line, that is, route AB in Figure 5a,b is similar to elastic-plastic material, and the strain can be understood as elastic strain (ε_{0t}^{el} , ε_{0c}^{el}) and non-elastic strain (ε_t^{ck} , ε_c^{in}). If damage occurs, the stress-strain route decreases according to the elastic modulus $(1-d)E_0$ of the stress peak secant after reduction, that is, route CD in Figure 5a,b is similar to elastic-plastic material, the compressive damage factor is expressed as d_c , the tensile damage factor is expressed as d_t , and the strain can be denoted by isotropic elastic damage (ε_t^{el} , ε_c^{el}) and isotropic plastic strain (ε_t^{pl} , ε_c^{pl}). The degradation curve of unloading stiffness under the specific compressive tension force is shown in Figure 8. The plastic parameters of the model are given default values, as shown in Table 8.

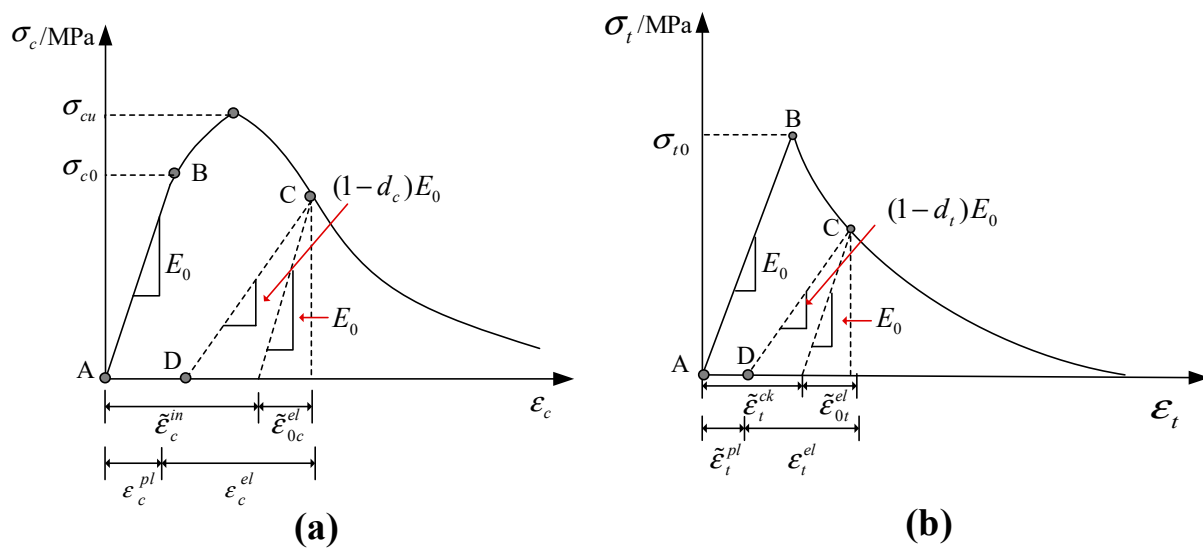


Figure 8. Unloading stiffness degradation curve under compressive tension of plastic damage model: (a) Degradation of unloading stiffness under pressure; (b) Degradation of unloading stiffness in the tensile state.

Table 8. Failure criteria parameter table of ABAQUS concrete plastic damage model.

ψ	ε	$\sigma_{b_0}/\sigma_{c_0}$	K_C	μ
30°	0.1	1.16	0.667	0.005

Notes: ψ —Expansion Angle; ε —Eccentricity; $\sigma_{b_0}/\sigma_{c_0}$ —Biaxial to uniaxial compressive strength ratio; K_C —K coefficient; μ —Viscosity coefficient.

4.2. Model Rationality Analysis

The model-building process is as follows: Firstly, all parts of the test piece are created in the Part module, including the beam, column, longitudinal bar, stirrup, etc. A three-dimensional Solid model is used for beams and columns, and three-dimensional Wire is used for longitudinal bars and stirrup. Then enter the Module list and click the Property module to input the constitutive model and section property of PVA fiber reinforced concrete and reinforcement material defined above, and then give the section property to the parts. Then, the Assembly function module is used to create an instance for each component, and the translation, array, rotation, and other operations are used to locate all entities in the overall coordinate system. The analysis step of this model adopts General Static analysis (Static, General). In order to avoid stress concentration, rigid pads are installed at the mid-beam loading point and the bottom of the column respectively, and reference points are created as Coupling points for the loading surface, as well as application points for displacement control loading. Use the Embedded command to embed rebar into PVA fiber concrete. The boundary condition of the bottom of the column is $U1 = U2 = U3 = UR1 = UR2 = UR3 = 0$. The set axial pressure load is applied at the loading point of the beam span, and the vertical load remains unchanged. The mesh size is 50 mm. Submit the job and finally view the analysis results in ABAQUS/Viewer. Through the above steps, the final model is shown in Figure 9.

From the frame structure test [27], it is known that the inter-mid-span displacement of the plain concrete frame gradually increases with the increase of structural load, and the trans-mid-strain, which reaches the inflection point at about 20 KN, in order to verify the rationality of the finite element model, the mid-span displacement and mid-span strain values under different loads of the prime concrete frame model are compared with the corresponding frame structure test results, and the comparison results are detailed in Figures 10 and 11.

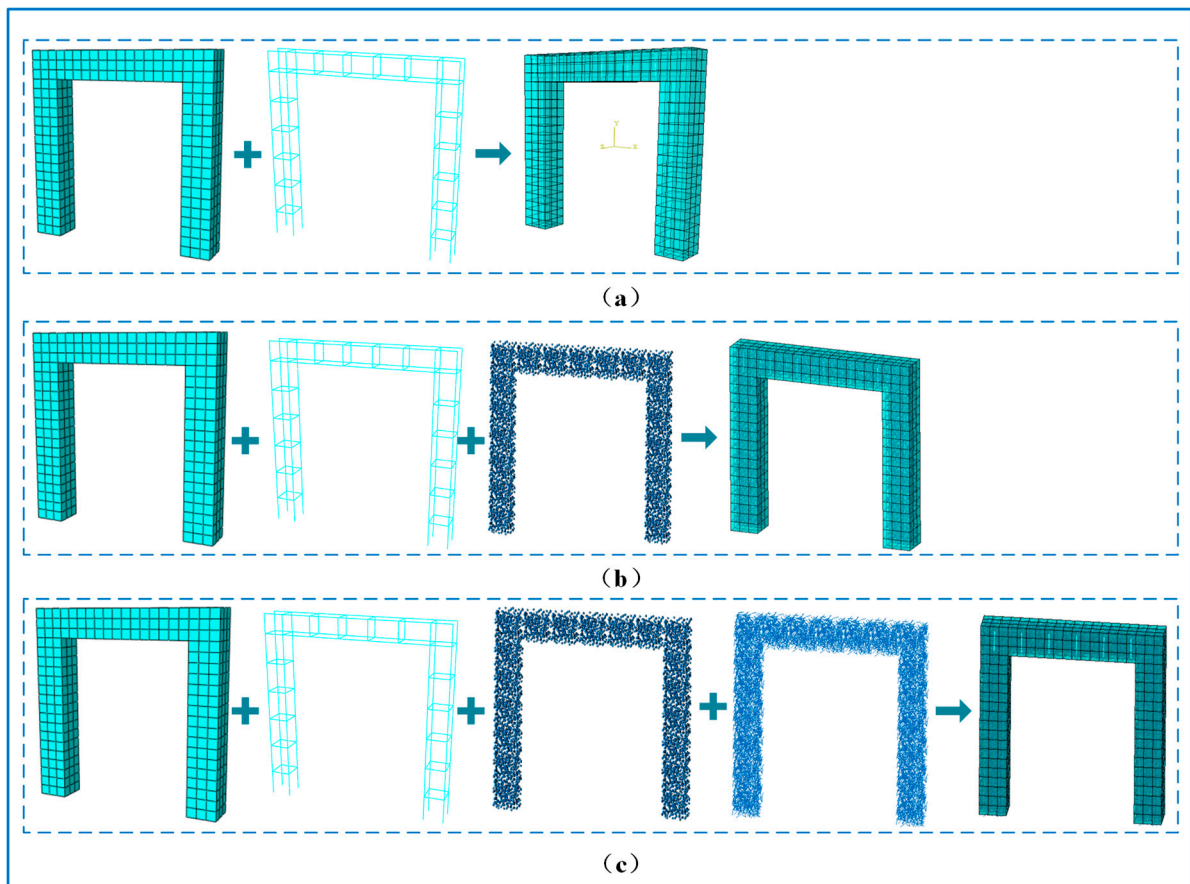


Figure 9. Finite element model of portal frame: (a) ordinary concrete frame model; (b) rubber concrete frame model; (c) PVA rubber concrete frame model.

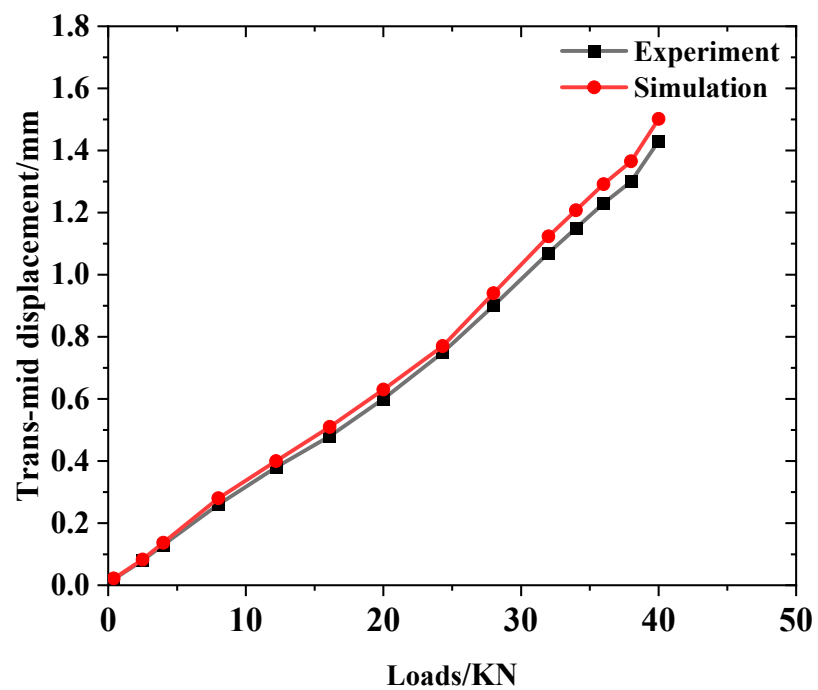


Figure 10. Numerical simulation of plain concrete frame and comparison of span displacement of frame structure test.

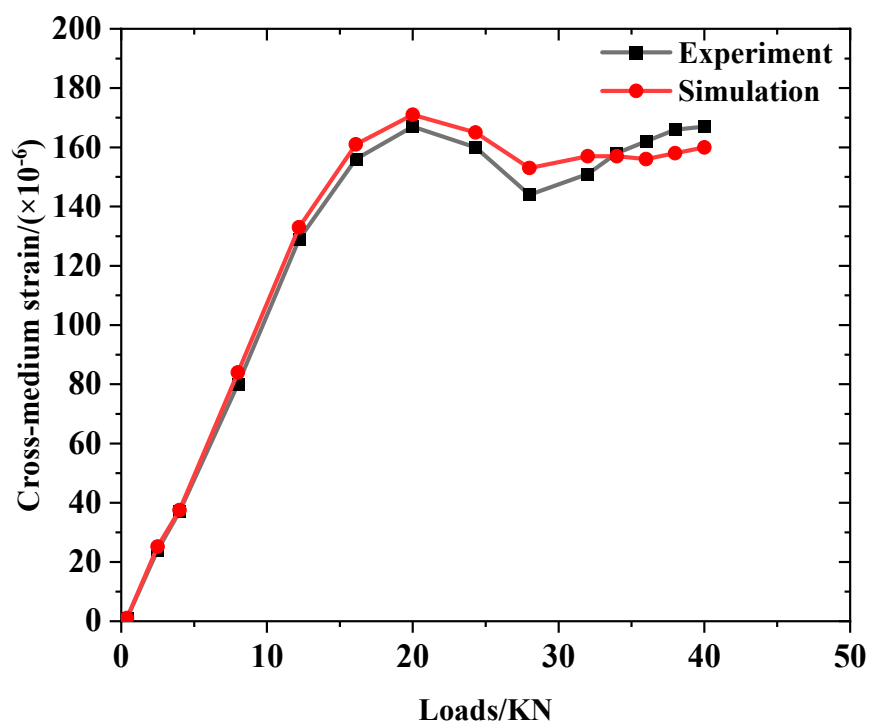


Figure 11. Numerical simulation of plain concrete frame and comparison of strain in the frame structure test.

Through the numerical simulation of ordinary concrete frame, it is obtained that the ordinary concrete load and span displacement are basically linear, and the simulated load-span mid-strainer curve results are compared with the experimental measured results, the deviation is within 5%, and the curve trend is basically the same. The numerical model of the established plain concrete frame is in good agreement with the frame structure test, which proves the rationality of the numerical model.

4.3. Analysis of Numerical Simulation Results

It is proposed to analyze four major types: ordinary concrete structure, rubber concrete structure, PVA fiber rubber concrete structure, and modified PVA fiber rubber concrete structure.

4.3.1. Displacement-Load Analysis of Frame Models

After ABAQUS analysis and calculation, the displacement clouds of the frame models of different materials under 20 KN load were taken respectively, as shown in Figure 12, from which it can be seen that the maximum displacement deformation of concrete and steel bars is located in the middle of the structural span. The relationship curve between the displacement and load of the four frame structures is shown in Figure 13, and it can be seen from the figure that the structural displacement of the rubber concrete frame model is larger than that of the ordinary concrete frame model, the main reason is that the appropriate amount of rubber can enhance the ductility of the concrete structure. Because PVA fiber plays the role of stiffener in rubber concrete, the displacement deformation of PVA rubber concrete frame model is smaller than that of rubber concrete frame model. On this basis, the addition of modifier can improve the poor interface compatibility between rubber particles and PVA fiber, and further reduce the displacement deformation of the modified PVA rubber concrete frame model.

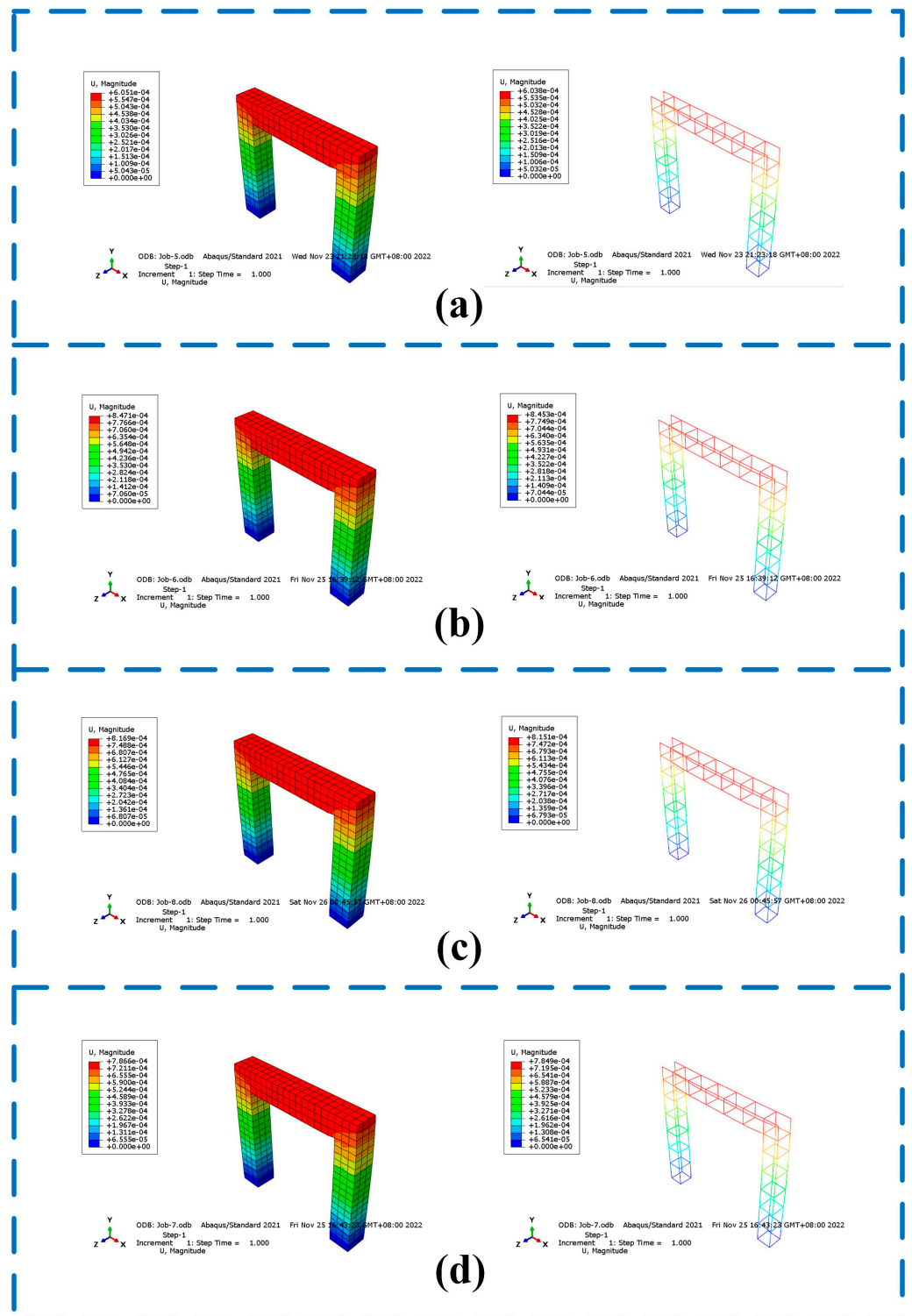


Figure 12. Displacement clouds of four frame structures: (a) ordinary concrete frame model; (b) rubber concrete frame model; (c) PVA rubber concrete frame model; (d) modified PVA rubber concrete frame model.

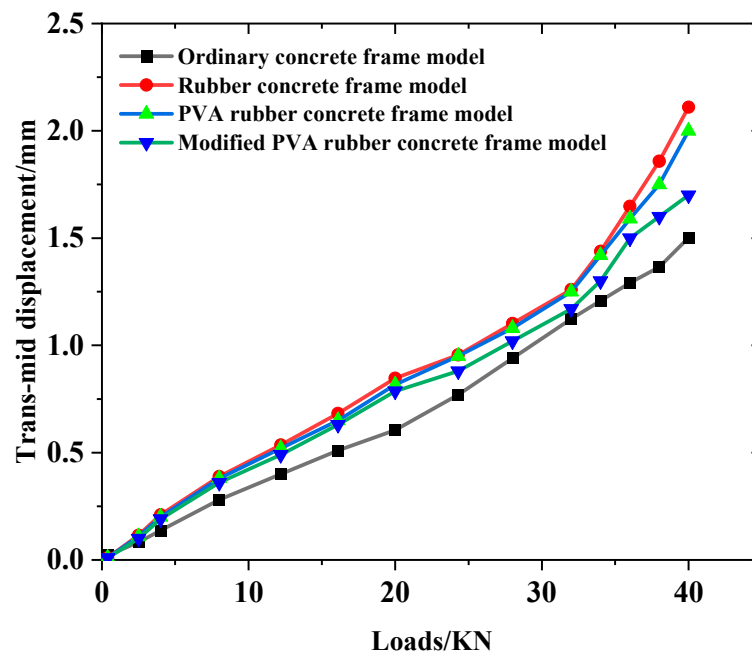


Figure 13. Relationship curve between displacement and load across four frame structures.

4.3.2. Strain–Load Analysis of Frame Model

After ABAQUS analysis and calculation, the strain cloud diagram of the frame model of different materials under 20 KN load was taken respectively, as shown in Figure 14, because the test load was applied by the jack to the middle and upper surface of the span, and the strain gauge was pasted in the middle of the span under the beam to measure the mid-center of the span, so the concrete matrix model in this paper took the strain in the E22 direction for analysis, and the steel model took the strain in the E11 direction for analysis. The stress in the E11 direction is mainly borne by the column, which is mainly compressed deformation at the beginning, and then the combined deformation of compression bending occurs, which bears greater stress and has a large strain. The strain of the column in the E22 direction model is much smaller than the strain in the span of the beam, which is the same as the test result. The relationship curve between strain and load in the span of the four frame structures is shown in Figure 15, the deformation capacity of rubber concrete is strong, under the same load, the rubber concrete frame model is larger than the ordinary concrete frame model, while the PVA fiber can improve the strain of the rubber concrete model, and the PVA fiber treated with modifier can further improve the model strain and its strength is further improved.

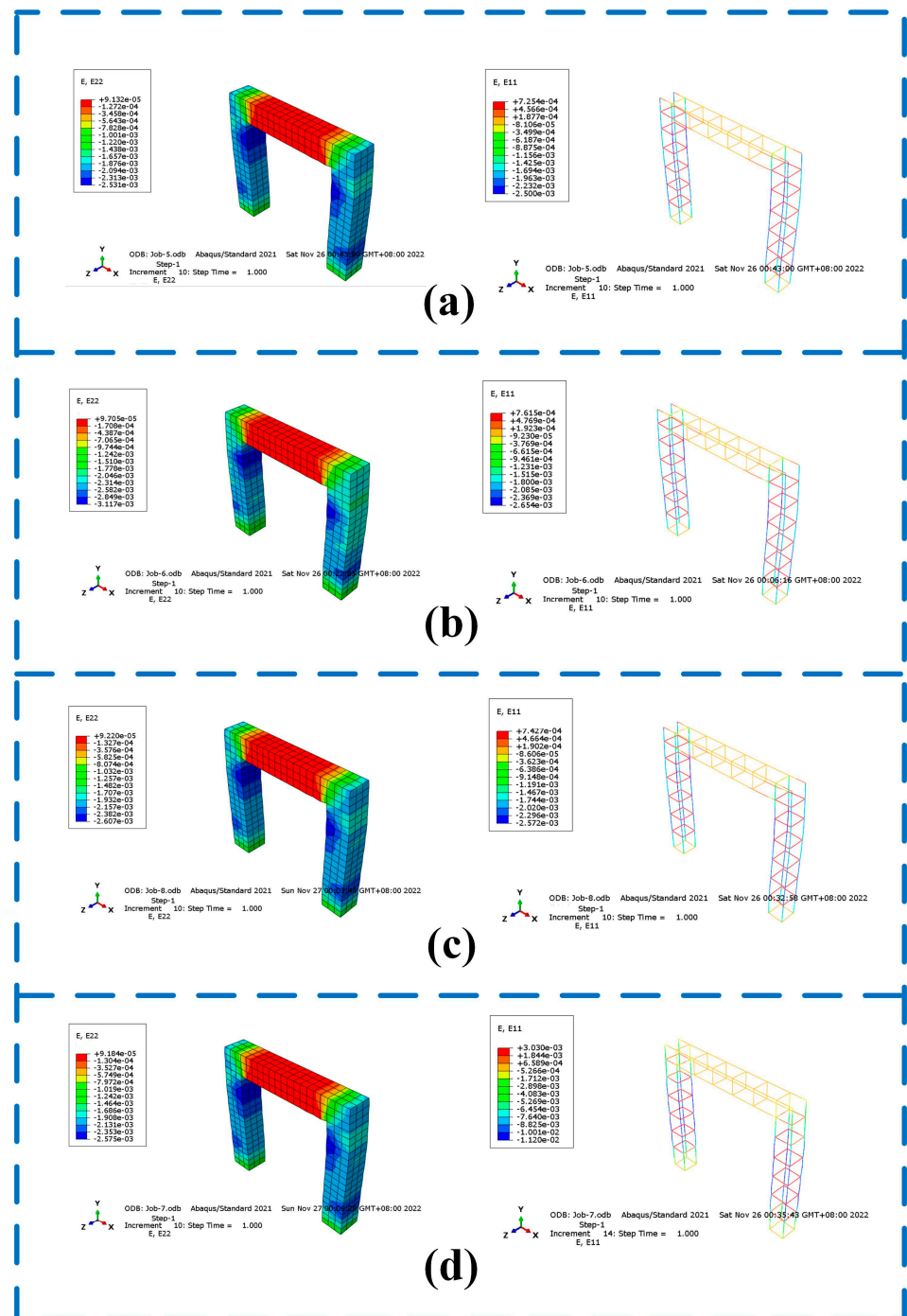


Figure 14. Strain cloud diagram of four frame structures: (a) ordinary concrete frame model; (b) rubber concrete frame model; (c) PVA rubber concrete frame model; (d) modified PVA rubber concrete frame model.

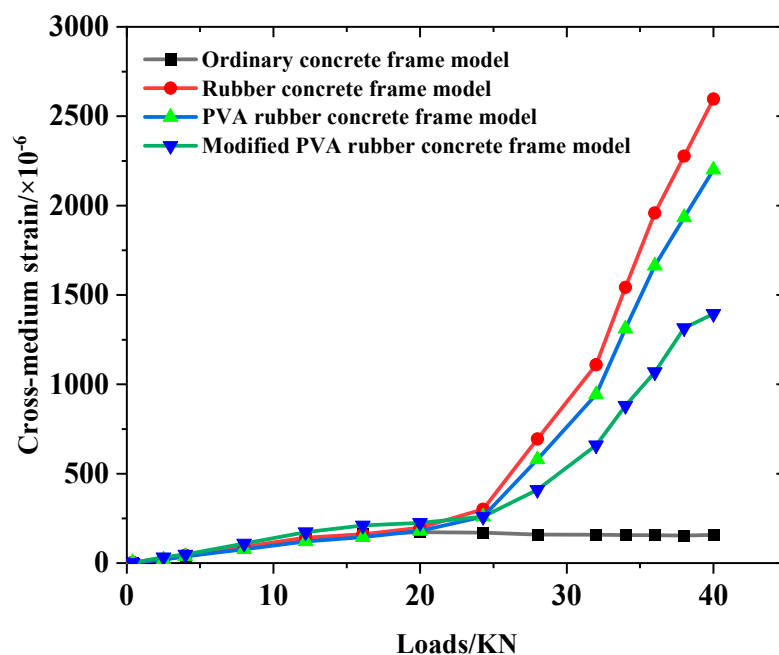


Figure 15. Relationship curves between strain and load in four frame structures.

5. Conclusions

In this paper, ABAQUS software is used to establish the door-shaped frame model of different materials, and the rationality of the model is verified by experiments, and the feasibility of modified PVA fiber rubber concrete in the frame structure is studied by model simulation. The main conclusions are as follows:

1. A suitable amount of PVA fiber can increase the strength of rubber concrete, decrease its brittleness, and increase its toughness, according to testing and analysis of the specimens' mechanical properties, such as compressive, flexural, and scanning electron microscopy. The bonding strength of the interface transition zone of the PVA fiber rubber concrete treated with KH560 is also improved, and the performance of the specimen is improved.
2. In the finite element frame model, the beam's mid-span strain is significantly more than the column's, the experimental conclusion and the failure of the frame construction both occur in the middle of the beam's span. By using numerical analysis, we investigate the viability of using rubber concrete in frame structures as a guide for future investigation.
3. The large deformation of rubber concrete can be improved with the use of PVA rubber concrete in concrete frame structures, and the use of PVA rubber concrete after KH560 modifier treatment can further improve structural strength and deformation. The proper use of the material can also lower costs while maintaining structural strength.

This study still needs to be further improved in the following two aspects: (1) PVA fiber rubber concrete has no special constitutive equation, this paper uses the fiber rubber concrete constitutive calculation first, and then we will explore the applicable constitutive equation for PVA fiber rubber concrete. (2) This paper only finished the simulation of the entire portal frame structure. In order to establish a rule, we can put up various rubber section sizes, PVA fiber rubber, and modified PVA fiber rubber models and test them in the beam–column junction region.

Author Contributions: Conceptualization, L.L.; methodology, Z.X.; software, F.X.; validation, Y.L., F.X., and W.C. (Wang Chen); investigation, W.C. (Wuxin Chen); resources, Z.X.; writing—original draft preparation, L.L. All authors have read and agreed to the published version of the manuscript.

Funding: This research was funded by Henan Provincial Development and Reform Commission (Grant No. Yufa Gaoji (2022) No. 315), 2021 Higher Education Teaching Reform Research and Practice Project in Henan Province (Grant No. 2021SJGLX670), Henan Province key research and development and promotion special (Grant No. 23B570003), the Innovative Funds Plan of Henan University of Technology (Grant No. 2020ZKCJ21), and the Zhengzhou Collaborative Innovation Project (Grant No. 21ZZXTCX09).

Institutional Review Board Statement: Not applicable.

Informed Consent Statement: Not applicable.

Data Availability Statement: Not applicable.

Conflicts of Interest: No potential conflicts of interest were reported by the authors.

References

1. Yunhong, H.; Lei, F.; Yan, H.; Hui, L.; Xule, T.; Qingli, H. Damage of rubber concrete under impact loads. *J. Vib. Shock*. **2019**, *38*, 73–80. [\[CrossRef\]](#)
2. Gesoğlu, M.; Güneyisi, E.; Khoshnaw, G.; İpek, S. Investigating properties of pervious concretes containing waste tire rubbers. *Constr. Build. Mater.* **2014**, *63*, 206–213. [\[CrossRef\]](#)
3. Ruochong, Y.; Zhiming, T.; Xiaoming, H.; Yiping, M. Research on Performance of Rubberized Concrete Incorporated with Polymer. *China J. Highw. Transp.* **2010**, *23*, 15–19. [\[CrossRef\]](#)
4. Gang, X.; Haojun, Z.; Sheng, X.; Liqiang, L. The uniaxia compression fatigue performance of rubber concrete. *Eng. Mech.* **2022**, *39*, 203–211. [\[CrossRef\]](#)
5. Khorrami, M.; Vafai, A.; Khalilitabas, A.; Desai, C.; Ardakani, M. Experimental Investigation on Mechanical Characteristics and Environmental Effects on Rubber Concrete. *Int. J. Concr. Struct. Mater.* **2010**, *4*, 17–23. [\[CrossRef\]](#)
6. Xu, J.; Yao, Z.Y.; Yang, G.; Han, Q.H. Research on crumb rubber concrete: From a multi-scale review. *Constr. Build. Mater.* **2020**, *232*, 117282. [\[CrossRef\]](#)
7. Yanli, H.; Peiwei, G.; Furong, L.; Aiqun, M.; Zhenpeng, Y. Experimental Study on Mechanical Properties of Rubber Concrete with Different Substitution Rates. *J. Build. Mater.* **2020**, *23*, 85–92. [\[CrossRef\]](#)
8. Zhenqian, L.; Yaru, Y.; Yong, X. Research review of fiber effect on properties of cement-based composite. *J. Text. Res.* **2021**, *42*, 177–183. [\[CrossRef\]](#)
9. Buyun, Y.; Jialiang, K.; Jing, S. Experimental research on freezing and thaw ing test of high ductile fiber concrete. *Concrete* **2017**, *11*, 114–118. [\[CrossRef\]](#)
10. Shiyong, J.; Shuai, T.; Weilai, Y.; Shijuan, W.; Tao, C. Mechanical Performance and Size Effect of Engineered Cementitious Composite (ECC) Subjected to Uniaxial Compression. *Mater. Rep.* **2017**, *31*, 161–168+173. [\[CrossRef\]](#)
11. Pengyu, Z.; Houlin, W.; Ye, Z.; Wenhui, G. Experimental study on mechanical properties of hybrid fiber rubber concrete based on orthogonal experiment. *Compos. Sci. Eng.* **2021**, 73–77. [\[CrossRef\]](#)
12. Zhang, Z.Y.; Wang, S.Y.; Feng, J.L. Frictional behaviour of the interface between concrete and rubber: Laboratory shear test and its elastoplastic model. *Eng. Fract. Mech.* **2018**, *197*, 192–205. [\[CrossRef\]](#)
13. Yuan, B.; Chen, M.; Chen, W.; Luo, Q.; Li, H. Effect of Pile-Soil Relative Stiffness on Deformation Characteristics of the Laterally Loaded Pile. *Adv. Mater. Sci. Eng.* **2022**, *2022*, 4913887. [\[CrossRef\]](#)
14. Yuan, B.; Chen, W.; Zhao, J.; Li, L.; Liu, F.; Guo, Y.; Zhang, B. Addition of alkaline solutions and fibers for the reinforcement of kaolinite-containing granite residual soil. *Appl. Clay Sci.* **2022**, *228*, 106644. [\[CrossRef\]](#)
15. Yuan, B.; Chen, W.; Zhao, J.; Yang, F.; Luo, Q.; Chen, T. The Effect of Organic and Inorganic Modifiers on the Physical Properties of Granite Residual Soil. *Adv. Mater. Sci. Eng.* **2022**, *2022*, 1–13. [\[CrossRef\]](#)
16. Yuan, B.; Li, Z.; Chen, W.; Zhao, J.; Lv, J.; Song, J.; Cao, X. Influence of Groundwater Depth on Pile-Soil Mechanical Properties and Fractal Characteristics under Cyclic Loading. *Fractal Fract.* **2022**, *6*, 198. [\[CrossRef\]](#)
17. Shi, B.K.; Zhu, W.X.; Yang, H.F.; Liu, W.Q.; Tao, H.T.; Ling, Z.B. Experimental and theoretical investigation of prefabricated timber-concrete composite beams with and without prestress. *Eng. Struct.* **2020**, *204*. [\[CrossRef\]](#)
18. Xu, X.Q.; Liu, Y.Q.; He, J. Study on mechanical behavior of rubber-sleeved studs for steel and concrete composite structures. *Constr. Build. Mater.* **2014**, *53*, 533–546. [\[CrossRef\]](#)
19. Yang, F.; Feng, W.H.; Liu, F.; Jing, L.; Yuan, B.; Chen, D. Experimental and numerical study of rubber concrete slabs with steel reinforcement under close-in blast loading. *Constr. Build. Mater.* **2019**, *198*, 423–436. [\[CrossRef\]](#)
20. Wang, J.Q.; Dai, Q.L.; Si, R.Z. Experimental and Numerical Investigation of Fracture Behaviors of Steel Fiber-Reinforced Rubber Self-Compacting Concrete. *J. Mater. Civ. Eng.* **2022**, *34*. [\[CrossRef\]](#)
21. Han, Q.H.; Wang, Y.H.; Xu, J.E.; Xing, Y.; Yang, G. Numerical analysis on shear stud in push-out test with crumb rubber concrete. *J. Constr. Steel Res.* **2017**, *130*, 148–158. [\[CrossRef\]](#)
22. Wang, J.; Dai, Q.; Si, R.; Guo, S. Investigation of properties and performances of Polyvinyl Alcohol (PVA) fiber-reinforced rubber concrete. *Constr. Build. Mater.* **2018**, *193*, 631–642. [\[CrossRef\]](#)

23. Feng, Y.; Niu, Z.; Zhao, C.; Li, L. Compressive Test Investigation and Numerical Simulation of Polyvinyl-Alcohol (PVA)-Fiber-Reinforced Rubber Concrete. *Buildings* **2023**, *13*, 431. [[CrossRef](#)]
24. Li, L.; Wang, W.; Xu, Z.; Niu, Z.; Li, X.; Wang, Q. Mechanical Property Test and Finite Element Simulation Analysis of KH-560 Coupling Agent-Modified PVA Rubber Concrete. *Geofluids* **2022**, *2022*, 1–17. [[CrossRef](#)]
25. Li, Y.; Wu, Y.; Yang, Y.; Han, Z.; Wang, M. Study on structural properties of reinforced rubber aggregate concrete. *J. Beijing Univ. Technol.* **2008**, *34*, 1280–1285.
26. Li, H.; Zhu, H.; Zhu, X. Influence of beam containing rubber aggregate on seismic performance of a frame-shear wall structure. *J. Shenyang Univ.* **2013**, *25*, 149–155.
27. Houmin, L.; Limei, T.; Zhan, S. Application of rubber concrete in reinforced concrete frame structure. *Build. Struct.* **2019**, *49*, 123–126. [[CrossRef](#)]
28. Qihong, Z.; Shuo, D.; Han, Z.; Yong, Y. Stress-Strain Relations of Steel Fiber Reinforced Rubberized Concrete under Uniaxial Cyclic Compression. *J. Build. Mater.* **2022**, *25*, 789–797. [[CrossRef](#)]
29. Ying, Z.; Xilin, L.; Xuecheng, N. Stress-strain Behavior for High-strength Steel Fiber Reinforced Concrete under Tensile Loading. *Struct. Eng.* **2017**, *33*, 107–113+200. [[CrossRef](#)]

Disclaimer/Publisher’s Note: The statements, opinions and data contained in all publications are solely those of the individual author(s) and contributor(s) and not of MDPI and/or the editor(s). MDPI and/or the editor(s) disclaim responsibility for any injury to people or property resulting from any ideas, methods, instructions or products referred to in the content.